Letter

Developing the quantum-dot single-photon sources with excellent performance by coupling asymmetric microcavity

Xiang You[1] and Yu-Ming He[1,2,*]

[1]Hefei National Laboratory, University of Science and Technology of China, Hefei 230088, China
[2]Hefei National Research Center for Physical Sciences at the Microscale and School of Physical Sciences, University of Science and Technology of China, Hefei 230026, China

(Received 23 July 2024; accepted 20 December 2024; published 21 January 2025)

Semiconductor quantum dots (QDs) coupled with optical microcavities provide an excellent platform for generating high-performance single-photon sources. However, the current microcavity structures are difficult to solve the tradeoff between single-photon purity and indistinguishability without additional filtering, due to challenges in suppressing broad phonon sideband spectrum and two-photon emission in the practical experiments. To address these issues, we have developed a novel asymmetric microcavity that supports two nondegenerate polarized modes, both resonant with a single quantum dot. One cavity mode is broadband and is used for excitation to reduce two-photon emission intensity, while the other is narrowband and is used for collection to enhance the indistinguishability of single-photon sources. This asymmetric microcavity also has the ability to overcome at least half of the photon efficiency loss under polarization filtering. Moreover, our model has employed an excitation pulse that resonates with cavity modes eliminating spectral distortion of intracavity fields, and efficiently achieving deterministic population inversion of QDs compared to an elliptical cavity. Our scheme paves the way to develop the excellent performance single-photon sources with higher brightness, near-unity purity, and indistinguishability without any additional filtering in practical experiments.

DOI: 10.1103/PhysRevResearch.7.L012016

Introduction. Single photons are excellent candidates for implementing quantum information processing, such as quantum communication [1–3], photonic quantum computing [4,5], quantum-enhanced metrology [6], and quantum networks [7,8]. To achieve this, highly efficient single-photon sources are required that have near-unity indistinguishability and purity, and can be produced on demand. Self-assembled quantum dots (QDs) are a promising solid-state quantum emitter [9,10], including near-unity quantum efficiency and narrow spectrum lines, making QDs an ideal platform for developing single-photon sources. In recent years, significant progress has been made in high-performance solid-state single-photon sources based on QDs [11–17]. By coupling QDs to elliptical microcavities [16], the challenge of 50% efficiency loss under spatially orthogonal excitation-collection methods has been overcome. Additionally, employing open and tunable microcavities [17], the system efficiency of single-photon sources can be improved to up to 57%. Recently, the swing up of quantum emitter population (SUPER) scheme [18,19] can theoretically achieve complete population inversion by two red-detuned excitation pulses, and it avoids photon loss by eliminating the need for laser background filtering. High-performance single-photon sources have also been employed in quantum key distribution [20–22], boson sampling [23,24], heralded multiphoton entangled states [25–28], and solid-state quantum networks [29–31].

An ideal single-photon source should emit photons one at a time. In practical experiments, the pulsed resonant excitation schemes are used to eliminate dephasing noise and time jitter for single excitons. However, the single-photon purity is limited by the reexcitation process [32,33], which depends on the ratio of the temporal width of the excitation pulse to the radiative lifetime of single excitons [32]. Shortening the radiative lifetime is an important prerequisite for increasing the excitation repetition rates, which directly enhances the brightness of single-photon sources. On the other hand, ideal single-photon sources require the emitted photons to be indistinguishable at any time. Unfortunately, QDs interact with their local solid-state environment generating a phonon sideband with broadband spectrum, which reduces the indistinguishability of emitted photons. This process persists even at $T = 0$ K [34], although it can be mitigated by spectral filtering at the expense of reducing the system efficiency of single-photon sources.

QDs embedded in an optical microcavity can significantly enhance the spontaneous emission rates and extract efficiency of single-photon sources due to the Purcell-enhanced effect, while also naturally suppressing the phonon sideband spectrum especially in the high-Q cavity [34]. However, the high-Q cavity acts as a dispersion device, that stretches the incident pulse into a long-lived intracavity field, and further increases the intensity of two-photon emission. In a low-Q cavity, the temporal broadening of input laser pulse can be slowed down, but the cavity acts as a broadband filter, making

*Contact author: yuminghe@mail.ustc.edu.cn

Published by the American Physical Society under the terms of the Creative Commons Attribution 4.0 International license. Further distribution of this work must maintain attribution to the author(s) and the published article's title, journal citation, and DOI.

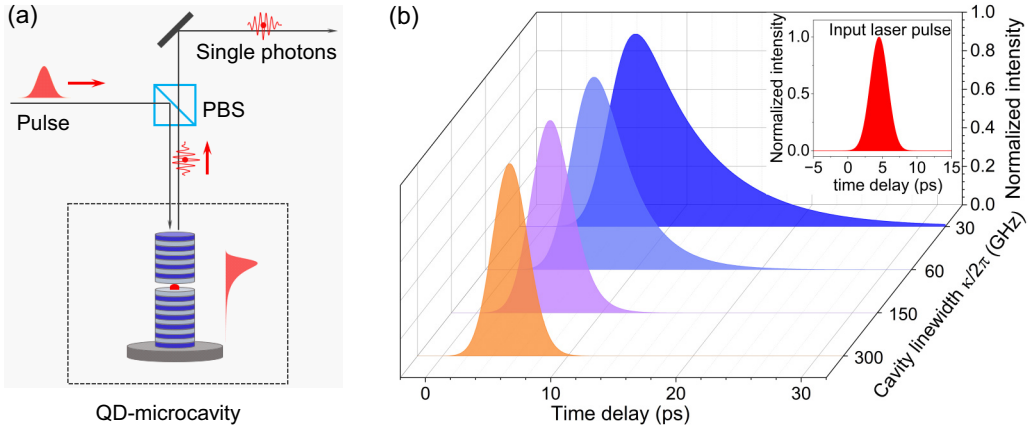


FIG. 1. (a) The schematic diagram of pulsed resonant excitation, QDs embedded in microcavities, and collecting the single photons under the spatially cross-polarized schemes. (b) The temporal line shape of intracavity fields as a function of linewidth of microcavities, with fixed the temporal width of Gaussian-shaped input pulse at 3 ps.

it harder to suppress the phonon sideband spectrum. This results in a tradeoff between the purity and indistinguishability of single-photon sources within microcavities.

To address these difficulties in solid-state single-photon sources, we propose a new design featuring asymmetric optical microcavities with two fundamental orthogonal polarization modes, both of which are resonate with a single QD. One cavity mode is broadband (low-Q factor), and acts as the excitation mode to reduce the intensity of two-photon emission. The other cavity mode is narrowband (high-Q factor), and used for collection to improve the indistinguishability of single-photon sources, that eliminates the tradeoff between single-photon purity and indistinguishability. Furthermore, the narrowband cavity mode provides a larger Purcell enhancement than broadband cavity mode for spontaneous emission process under the same mode volume. The design addresses the 50% efficiency loss in spatially orthogonal excitation-collection schemes, and improves the extraction efficiency of polarized single-photon sources. These asymmetric microcavities have the potential to create a perfect solid-state single-photon source with the high-efficiency, near-unity purity, and indistinguishability without any filtering in practical experiments, simultaneously.

Single-photon sources within microcavity. To develop high-performance single-photon sources, coupling a single QD into optical microcavities has been proposed as an advanced platform, as shown in Fig. 1(a). To analyze the temporal distribution of intracavity fields, a laser pulse with a Gaussian-shaped envelope function $\varepsilon_{in}(t)$ is injected into the microcavities, as shown in the insets of Fig. 1(b), with a fixed pulse width of 3 ps. The intracavity fields $\alpha(t)$ can be calculated by solving the quantum Langevin equations $\partial_t\alpha(t) = -\frac{\kappa}{2}\alpha(t) + \sqrt{\kappa}\varepsilon_{in}(t)$, where κ is the decay rate of microcavities. Figure 1(b) shows the normalized intensity of intracavity fields $I(t) = |\alpha(t)|^2$ at different linewidths of microcavities. A significant temporal broadening is observed, accompanied by a longer time delay at the linewidth of 30 GHz. The temporal broadening gradually slows down as the linewidth of optical microcavities increases. At a linewidth of 300 GHz, the temporal profile of intracavity fields closely resembles the input laser pulse, suggesting that the temporal broadening of laser pulse disappears when the linewidth of microcavities is large enough.

For a symmetric microcavity with two degenerate polarization cavity modes, we model QDs as a two-level system, resonantly coupled to a classical intracavity field $\alpha(t)$ and a cavity mode with annihilation operator a. The interaction Hamiltonian of QDs cavity can be expressed as follows:

$$H_{sy} = \hbar g\alpha(t)(\sigma + \sigma^\dagger) + \hbar g(a\sigma^\dagger + a^\dagger\sigma), \tag{1}$$

where σ is the lowering operator of two-level system and g is coupling constant between two-level system and cavity. Here, we consider the natural radiative decay rate of two-level system of $\gamma = 2\pi \times 0.3\,\mathrm{GHz}$ [17]. Enhancing the extract efficiency of single photons and reducing spontaneous radiative lifetime both require the Purcell acceleration through the optical microcavities. In our simulation, we fix the Purcell factor of $F_p = 9$, enabling us to calculate the coupling constant as $g = \sqrt{F_p\kappa\gamma}/2$.

Figure 2 shows the excitation-emission process of a two-level system within one pulse excitation cycle. At initial time t_0, the system remains at the ground state (I). Upon the arrival of the pulse, it is transferred to the excited state (II) with a probability of P_1. After a duration t_1 of intracavity fields, it subsequently decays to ground state (III) at t_2, and emits a photon into cavity modes with a probability of $\beta = F_p/(1 + F_p)$. During one pulse cycle, there exists a finite probability P_2 for the two-level system to be excited again due to the residual intracavity fields, as shown in Fig. 2(a)(IV). This results in the emission of a second photon into cavity modes with the same probability of β at t_4. While there exist three or more photons emission processes, the probabilities are much lower. Therefore, we simply consider the two-photon emission during the one pulse excitation cycle. Simultaneously, due to the finite storage time of microcavities, there is an allowed coherence exchange of photons between the two-level system and the cavity modes, determined by the interaction Hamiltonian terms of $\hbar g(a\sigma^\dagger + a^\dagger\sigma)$. After process (III), a photon emitted into cavity modes can be reabsorbed by the two-level system with a probability of P_{ce} before it escapes from the microcavities at t_3, and returns to the excited state again, as shown in Fig. 2(b)(IV). It subsequently redecays to the ground state at

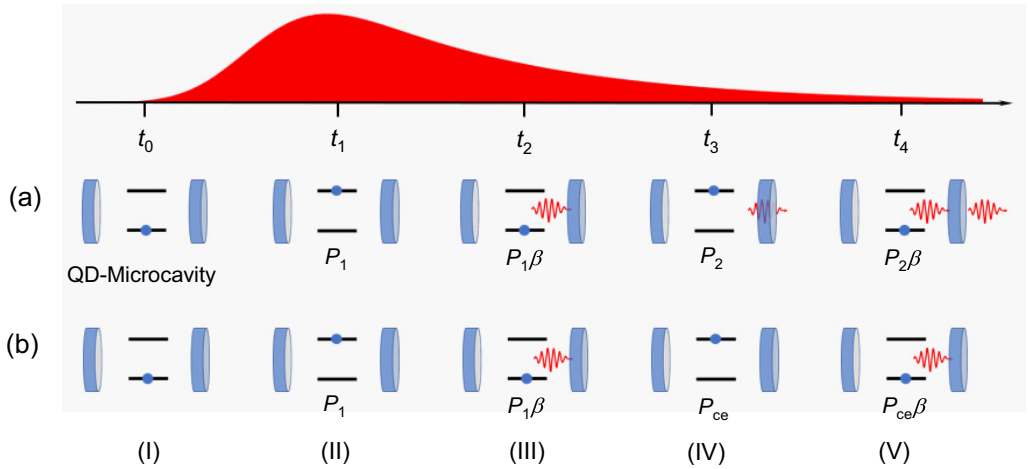


FIG. 2. (a) Two-photon emission and (b) coherence exchange process for the two-level system couples with microcavity. Under the pulsed resonant excitation: two-level system is transferred from ground state (I) to excited state (II) with a probability of P_1, (III) then decay to the ground state when intracavity fields duration at t_2 and emits a photon into cavity modes with a probability of β; (IV) Subsequently, the two-level system has a finite probability to absorb a photon that from intracavity fields (a) or emitted photon (b), and returns to the excited state again at t_3; (V) Repeating the process (III), the two-level system secondly decays to the ground state and emits a photon into cavity modes again when the intracavity fields duration at t_4, there are two (one) emitted photons into cavity modes for (a) and (b) under the one pulse excitation cycle.

t_4, ensuring there is no more than one photon in the cavity modes. Thus, the coherence exchange process does not affect the single-photon purity. Although the two-photon emission and coherence exchange occur independently, they compete with each other due to the common excited-state energy level. Within one pulse excitation cycle, the mean photon number $n_\sigma(n_a)$ that decays from the two-level system (cavity modes) are

$$n_\sigma = P_1 + P_{ce} + P_2, \tag{2a}$$

$$n_a = P_1\beta - P_{ce}(1-\beta) + P_2\beta. \tag{2b}$$

The second-order correlation function of single-photon sources can be written by the photon number probability p_n using the relation [33]:

$$g^{(2)}(0) = \frac{\sum_n n(n-1)p_n}{\left(\sum_n np_n\right)^2}. \tag{3}$$

Here, the probability of emitting more than two photons is small enough to be negligible, which allows for a good approximation as $g^{(2)}(0) = \frac{2p_2}{(p_1+2p_2)^2}$. In our model, $p_1 + 2p_2 = n_a$ represents the mean photon number that decay from the cavity modes, and the probability of two photons decay from the cavity modes during a single pulse cycle is given by $p_2 = P_2\beta^2$. As a result, the residual second-order correlation function of single-photon sources extracted from cavity modes is

$$g^{(2)}(0) = \frac{2P_2}{n_a^2}\beta^2. \tag{4}$$

To analyze the purity of single photons, we utilized the PYTHON package QUTIP to solve the Lindblad master equation [35,36], based on the Hamiltonian described in Eq. (1). This enabled us to extract simulated results for $n_\sigma = (1+F_p)\int \gamma\langle\sigma^\dagger\sigma\rangle dt$ and $n_a = \int \kappa\langle a^\dagger a\rangle dt$. Under the π-pulse resonant excitation, the two-level system is deterministically prepared in the excited state, i.e.,$P_1 = 1$. From this state, we can calculate the probability $P_2(P_{ce})$ of two-photon emission (coherence exchange), and plotted it as a function of the linewidth $\kappa/2\pi$ of optical microcavities in Fig. 3(a). In the range of $\kappa/2\pi < 150$ GHz, the probability of two-photon emission rapidly decreases, and gradually tends to flat when $\kappa/2\pi$ is larger than 150 GHz. This results in a reduction in the residual second-order correlation of single-photon sources, as shown in Fig. 3(b). Eventually, the probability of two-photon emission converges to a limit value that is determined by the initial width of the Gaussian-shaped input pulse. Meanwhile, the probability of coherence exchange decreases as the linewidth of microcavities increases and eventually vanishes in the bad-cavity limit, i.e., $g \ll \kappa$. This occurs because the rate at which emitted photons escape from microcavities exceeds the rate at which they are absorbed by the two-level system.

Asymmetric microcavities. Based on the numerical results that presented in Fig. 3, it is clear that the single-photon purity can be improved by increasing the linewidth of optical microcavities. However, the spontaneous emission noise such as phonon sideband, can degrade the indistinguishability of single-photon sources in practical experiments. Reference [34] indicates that phonon sideband spectrum can be suppressed by the high-Q cavity. The simulation results show that increasing the linewidth of microcavities from 30–300 GHz reduces the single-photon indistinguishability from 0.99 to 0.94. Thus, there exists a tradeoff between the purity and indistinguishability of single-photon sources within microcavities. Furthermore, when QDs are coupled to microcavities with two degenerate polarized modes, that results in a loss of at least half of the system efficiency of single photons under the polarization filtering.

To address these challenges, we propose a novel asymmetric microcavity with two nondegenerate polarized modes, both of which are resonant with a single QD, as shown in Fig. 4. The V-polarized cavity mode is broadband and serves

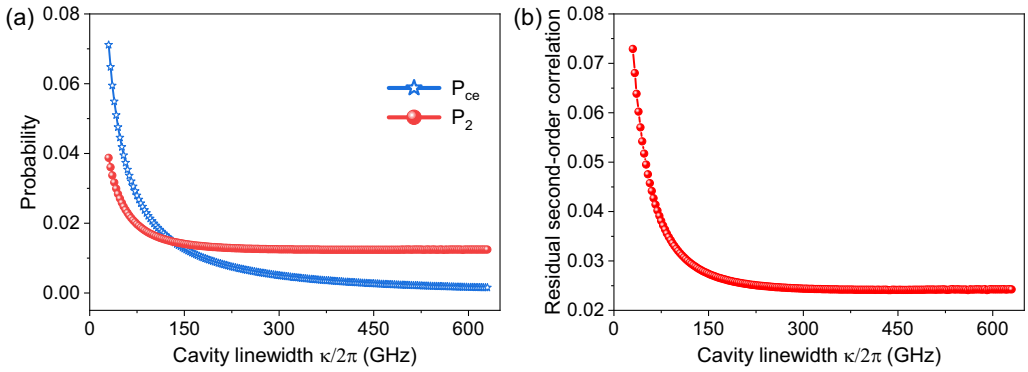


FIG. 3. The numerical results for QDs coupled to symmetric microcavities. Under the π-pulse resonant excitation, (a) the probability of two-photon emission (red line) and coherence exchange (blue line) as a function of linewidth of microcavities, (b) residual second-order correlation values $g^{(2)}(0)$ as a function of linewidth of microcavities.

as an excitation by modulating the polarization of the laser pulse. The red shadow area in Fig. 4 represents the intracavity fields, generated by a resonant Gaussian-shaped laser pulse (gray shadow area). The spectral line shape is a symmetric profile in the frequency domain, which helps to achieve the deterministic population inversion of QDs compared to the detuned laser pulse [35]. In contrast, the H-polarized cavity mode is narrowband and optimized for collection. It effectively suppresses the spontaneous radiation noise spectrum, thereby enhancing the indistinguishability of single-photon sources in practical experiments.

Based on the model that a single QD is coupled to asymmetric microcavity using excitation-collection methods, the interaction Hamiltonian can be represented as follows:

$$H_{\text{asy}} = \hbar g(a_H\sigma^\dagger + a_H^\dagger\sigma) + \hbar g(a_V\sigma^\dagger + a_V^\dagger\sigma) + \hbar g\alpha_V(t)(\sigma + \sigma^\dagger), \tag{5}$$

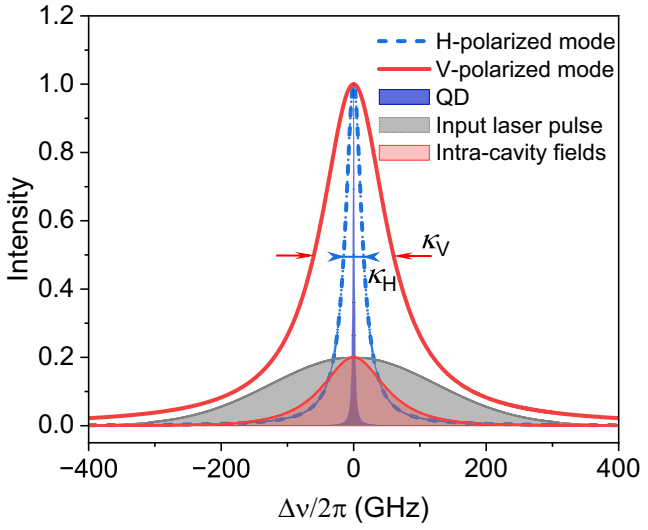


FIG. 4. The schematic diagram of asymmetric microcavities with two fundamental orthogonal polarization modes and resonant with single QD in the frequency domain. The V-polarized cavity mode is broadband and is used for excitation (red line), the H-polarized cavity mode is narrowband and is used for collection (blue dotted line), and the red area represents the intracavity fields.

where $a_H(a_V)$ represents the annihilation operator of H-polarized (V-polarized) cavity mode, respectively. To maintain the same radiative lifetime of QDs in the asymmetric microcavity, the Purcell factor of $F_p = 9$ is fixed in the simulation, which allows us to calculate the coupling coefficient $g = \frac{1}{2}\sqrt{F_p\gamma/(\frac{1}{\kappa_H} + \frac{1}{\kappa_V})}$, and further to get the Purcell factor of H-polarized (V-polarized) cavity mode of $F_{H(V)} = \frac{F_p}{1+\kappa_{H(V)}/\kappa_{V(H)}}$. The extraction efficiency of polarized single-photon sources from H-polarized (V-polarized) cavity mode is $\beta_{H(V)} = \frac{F_{H(V)}}{1+F_p}$ respectively. We plot $\beta_{H(V)}$ as a function of linewidth $\kappa_V/2\pi$ for V-polarized cavity mode, while fixing the linewidth of H-polarized cavity mode at $\kappa_H/2\pi = 30\,\text{GHz}$, as shown in Fig. 5(a). Due to the asymmetric Purcell enhancement for two polarized cavity modes, the extract efficiency of H-polarized single photons significantly surpasses 50%, while V-polarized single photons are suppressed simultaneously. This characteristic makes asymmetric microcavities an excellent approach for achieving high-efficiency polarized single-photon sources under cross-polarization schemes, highlighting one of the key advantages of asymmetric microcavities.

Another advantage of asymmetric microcavities is their ability to eliminate the tradeoff between purity and indistinguishability of single-photon sources. In order to analyze the purity of polarized single-photon sources, it is essential to determine the mean photon number n_σ, n_{aH}, and n_{aV}, which decay from a two-level system, H-polarized and V-polarized cavity mode, respectively. These values are calculated as follows:

$$n_\sigma = P_1 + P_{cH} + P_{cV} + P_2, \tag{6a}$$

$$n_{aH} = P_1\beta_H - P_{cH}(1-\beta_H) + P_{cV}\beta_H + P_2\beta_H, \tag{6b}$$

$$n_{aV} = P_1\beta_V - P_{cV}(1-\beta_V) + P_{cH}\beta_V + P_2\beta_V. \tag{6c}$$

We utilized the PYTHON package QUTIP to solve the Lindblad master function based on the Hamiltonian described in Eq. (5). Under π-pulse resonant excitation, the two-level system is deterministically prepared in the excited state, i.e., $P_1 = 1$. This allows us to calculate the probabilities P_2, $P_{cH}(P_{cV})$ of two-photon emission, coherence exchange within H-polarized (V-polarized) cavity mode, respectively. Moreover, the probability of two photons extracted from the H-polarized (V-polarized) cavity modes during a single pulse

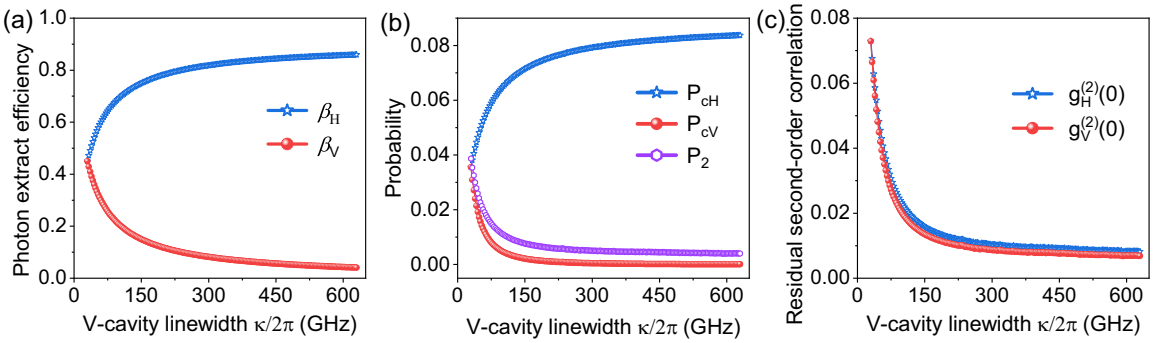


FIG. 5. The numerical results for QDs couple into asymmetric microcavity. Under the π-pulse resonant excitation, (a) the extract efficiency $\beta_H(\beta_V)$ of H-polarized (V-polarized) single-photon sources as a function of linewidth of V-polarized cavity mode. (b) The probability of two-photon emission (purple line) and coherence exchange within H-polarized (V-polarized) cavity mode [blue (red) line] as a function of linewidth of V-polarized cavity mode. (c) Residual second-order correlation values $g^{(2)}_{H(V)}(0)$ as a function of linewidth of V-polarized cavity mode.

cycle is given by $p_{2H(V)} = P_2\beta^2_{H(V)}$. These values enable the determination of the residual second-order correlation values of the polarized single-photon sources as:

$$g_H^{(2)}(0) = \frac{2P_2}{n_{aH}^2}\beta_H^2, \tag{7a}$$

$$g_V^{(2)}(0) = \frac{2P_2}{n_{aV}^2}\beta_V^2. \tag{7b}$$

Figure 5(b) depicts the probabilities P_2 and $P_{cH(V)}$ as a function of linewidth of V-polarized cavity mode, respectively. Figure 5(c) shows the residual second-order correlation values $g^{(2)}_{H(V)}(0)$ of H-polarized and V-polarized single-photon sources. It is evident that in asymmetric microcavity, the residual second-order correlation values $g^{(2)}_{H(V)}(0)$ are lower than $g^{(2)}(0)$ in symmetric microcavity at the same linewidth. This reduction is attributed to the larger probability P_{cH} of coherence exchange of photons between H-polarized cavity mode and two-level system in asymmetric cavity compared to P_{ce} in symmetric cavity. This suppresses the two-level system absorption of photons from intracavity fields and prevents the emission of a second photon into the cavity modes, eventually leading to a decrease in the two-photon emission intensity within one pulse excitation cycle.

For our asymmetric microcavity with $\kappa_{H(V)}/2\pi = 30(300)\,\mathrm{GHz}$, compared to the symmetric microcavity at the linewidth of 300 GHz, the extraction efficiency of H-polarized single-photon sources increases by ∼1.8 times and the residual second-order correlation values decrease by ∼2.4 times. Additionally, efficient suppression of the phonon sideband spectrum enhances the single-photon indistinguishability from 0.94 to 0.99 as referenced in Ref. [34]. On the other hand, the elliptical microcavities can also overcome 50% efficiency loss for polarized single-photon sources. However, similar to a symmetric microcavity, it cannot simultaneously suppress the temporal broadening of input pulse and phonon sideband noise. Under the same Purcell enhancement and extract efficiency as the asymmetric microcavity, where, the linewidth of elliptical microcavity is $\kappa_{H(V)}/2\pi = 30\,\mathrm{GHz}$ and mode splitting is $\Delta_{HV}/2\pi = 45\,\mathrm{GHz}$, the intensity of two-photon emission from QDs is ∼7 times greater than in asymmetric microcavity. Moreover, our schemes utilize the resonant laser pulse with cavity modes, which avoid spectral distortion of intracavity fields, and achieve deterministic population inversion of QDs more efficiently compared to elliptical microcavity protocols [35] or other nonresonant excitation protocols served for QD microcavities, such as the SUPER scheme [18,19] or two-color pulse excitation [15].

Furthermore, it is important to point out that the asymmetric microcavity enables frequency detuning between the broadband cavity mode and narrow cavity mode, which does not significantly affect the properties of single photons but only influences the required π-pulse power. This detuning could also slightly enhance the extraction efficiency of polarized single-photon sources. Additionally, by using the broadband cavity mode, the spectral distortion of intracavity fields caused by the nonresonant input pulse is effectively reduced. As a result, the asymmetric microcavities are compatible with various excitation strategies. Finally, we present two feasible approaches to achieve an asymmetric optical cavity with both low-Q and high-Q fundamental cavity modes simultaneously, although they may have some technical challenges. The first method involves utilizing the different refractive indices of cavity mirrors for H-polarized and V-polarized light, which induces the bandwidth differences for the two fundamental cavity modes. The second method is to increase the decay rate of one cavity mode by introducing imperfections along the corresponding cavity axis, which can also create the desired asymmetry in the optical cavity.

Conclusions. In summary, our asymmetric microcavities offer an excellent solution to generate high-performance solid-state single-photon sources. They combine the benefits of narrowband and broadband cavity modes, effectively suppressing the spontaneous emission noise spectrum and minimizing intensity of two-photon emission. Furthermore, these eliminate the tradeoff between single-photon purity and indistinguishability. Additionally, the asymmetric structure enables unequal Purcell enhancement for two orthogonal polarization cavity modes, effectively overcoming the 50% efficiency loss under the spatially orthogonal excitation-collection methods. Moreover, the asymmetric microcavities can be applied to a variety of excitation protocols, such as resonant excitation, SUPER scheme, and two-color excitation.

By optimizing the system parameters of QDs couple to asymmetric microcavities, we can establish an outstanding platform for generating on-demand single-photon sources with higher brightness and system efficiency. These sources exhibit near-unity purity and indistinguishability without requiring additional filtering in practical experiments, paving the way for broader applications in quantum information processing and long-distance quantum networks.

Acknowledgments. The authors would like to thank Prof. Chao-Yang Lu, Dr. Jian Qin, Geng-Yan Zou, and Run-Ze Liu for fruitful discussion and suggestions. This work is supported by the Innovation Program for Quantum Science and Technology (2021ZD0301400), Youth Innovation Promotion Association CAS (No. Y2023128), and funded by Anhui Postdoctoral Scientific Research Program Foundation (No. 2024C890).

[1] J.-W. Pan, Z.-B. Chen, C.-Y. Lu, H. Weinfurter, A. Zeilinger, and M. Zukowski, Multiphoton entanglement and interferometry, Rev. Mod. Phys. **84**, 777 (2012).

[2] C.-Y. Lu, Y. Cao, C.-Z. Peng, and J.-W. Pan, Micius quantum experiments in space, Rev. Mod. Phys. **94**, 035001 (2022).

[3] Y.-A. Chen, Q. Zhang, T.-Y. Chen *et al.*, An integrated space-to-ground quantum communication network over 4,600 kilometres, Nature (London) **589**, 214 (2021).

[4] P. Kok, W. J. Munro, K. Nemoto, T. C. Ralph, J. P. Dowling, and G. J. Milburn, Linear optical quantum computing with photonic qubits, Rev. Mod. Phys. **79**, 135 (2007).

[5] S. Aaronson and A. Arkhipov, The computational complexity of linear optics, Theor. Comput. **9**, 143 (2013).

[6] S. Slussarenko, M. M. Weston, H. M. Chrzanowski, L. K. Shalm, V. B. Verma, S. W. Nam, and G. J. Pryde, Unconditional violation of the shot-noise limit in photonic quantum metrology, Nat. Photon. **11**, 700 (2017).

[7] P. Lodahl, Quantum-dot based photonic quantum networks, Quantum Sci. Technol. **3**, 013001 (2018).

[8] C.-Y. Lu and J.-W. Pan, Quantum-dot single-photon sources for the quantum internet, Nat. Nanotechnol. **16**, 1294 (2021).

[9] P. Senellart, G. Solomon, and A. White, High-performance semiconductor quantum-dot single-photon sources, Nat. Nanotechnol. **12**, 1026 (2017).

[10] I. Aharonovich, D. Englund, and M. Toth, Solid-state single-photon emitters, Nat. Photon. **10**, 631 (2016).

[11] A. V. Kuhlmann, J. H. Prechtel, J. Houel, A. Ludwig, D. Reuter, A. D. Wieck, and R. J. Warburton, Transform-limited single photons from a single quantum dot, Nat. Commun. **6**, 8204 (2015).

[12] N. Somaschi, V. Giesz, L. D. Santis, J. C. Loredo, M. P. Almeida, G. Hornecker, S. L. Portalupi, T. Grange, C. Antón, J. Demory, C. Gómez, I. Sagnes, N. D. Lanzillotti-Kimura, A. Lemaítre, A. Auffeves, A. G. White, L. Lanco, and P. Senellart, Near-optimal single-photon sources in the solid state, Nat. Photon. **10**, 340 (2016).

[13] X. Ding, Y. He, Z.-C. Duan, N. Gregersen, M.-C. Chen, S. Unsleber, S. Maier, C. Schneider, M. Kamp, S. Höfling, C.-Y. Lu, and J.-W. Pan, On-demand single photons with high extraction efficiency and near-unity indistinguishability from a resonantly driven quantum dot in a micropillar, Phys. Rev. Lett. **116**, 020401 (2016).

[14] F. Liu, A. J. Brash, J. O'Hara, L. M. P. P. Martins, C. L. Phillips, R. J. Coles, B. Royall, E. Clarke, C. Bentham, N. Prtljaga, I. E. Itskevich, L. R. Wilson, M. S. Skolnick, and A. M. Fox, High purcell factor generation of indistinguishable on-chip single photons, Nat. Nanotechnol. **13**, 835 (2018).

[15] Y.-M. He, H. Wang, C. Wan, M.-C. Che, X. Ding, J. Qin, Z.-C. Duan, S. Chen, J.-P. Li, R.-Z. Liu, C. Schneider, M. Atatüre, S. Höfling, C.-Y. Lu, and J.-W. Pan, Coherently driving a single quantum two-level system with dichromatic laser pulses, Nat. Phys. **15**, 941 (2019).

[16] H. Wang, Y.-M. He, T.-H. Chung, H. Hu, Y. Yu, Si Chen, X. Ding, M.-C. Chen, J. Qi, X.-x. Yang, R.-Z. Liu, Z.-C. Duan, J.-P. Li, S. Gerhardt, K. Winkler, J. Jurka, L.-J. Wang, N. Gregersen, Y.-H. Hu, Q. Dai, S.-y Yu, S. Höfling, C.-Y. Lu , and J.-W. Pan, Towards optimal single-photon sources from polarized microcavities, Nat. Photon. **13**, 770 (2019).

[17] N. Tomm, A. Javadi, N. O. Antoniadis, D. Najer, M. C. Löbl, A. R. Korsch, R. Schott, S. R. Valentin, A. D. Wieck, A. Ludwig, and R. J. Warburton, A bright and fast source of coherent single photons, Nat. Nanotechnol. **16**, 399 (2021).

[18] T. K. Bracht, M. Cosacchi, T. Seidelmann, M. Cygorek, A. Vagov, V. M. Axt, T. Heinde, and D. E. Reiter, Swing-up of quantum emitter population using detuned pulses, PRX Quantum **2**, 040354 (2021).

[19] Y. Karli, F. Kappe, V. Remesh, T. K. Bracht, J. Münzberg, S. C. da Silva, T. Seidelmann, V. M. Axt, A. Rastelli, D. E. Reiter, and G. Weihs, Super scheme in action: Experimental demonstration of red-detuned excitation of a quantum emitter, Nano Lett. **22**, 6567 (2022).

[20] E. Waks, K. Inoue, C. Santori, D. Fattal, J. Vuckovic, G. S. Solomon, and Y. Yamamoto, Quantum cryptography with a photon turnstile, Nature (London) **420**, 762 (2002).

[21] M. Zahidy, M. T. Mikkelsen, R. Müller, B. D. Lio, M. Krehbiel, Y. Wang, N. Bart, A. D. Wieck, A. Ludwig, M. Galili, S. Forchhammer, P. Lodahl, L. K. Oxenløwe, D. Bacco, and L. Midolo, Quantum key distribution using deterministic single-photon sources over a field-installed fibre link, Npj Quantum Inf. **10**, 2 (2024).

[22] Jingzhong Yang, Z.-h Jiang, F. Benthin, J. Hanel, T. Fandrich, R. Joos, S. Bauer, S. Kolatschek, A. Hreibi, E. P. Rugeramigabo, M. Jetter, S. L. Portalupi, M. Zopf, P. Michler, S. Kück, and F. Ding, High-rate intercity quantum key distribution with a semiconductor single-photon source, Light: Sci. Appl. **13**, 150 (2024).

[23] H. Wang, Y. He, Y.-H. Li, Z.-E. Su, B. Li, H.-L. Huang, X. Ding, M.-C. Chen, C. Liu, J. Qin, J.-P. Li, Y.-M. He, C. Schneider, M. Kamp, C.-Z. Peng, S. Höfling, C.-Y. Lu, and J.-W. Pan, High-efficiency multiphoton boson sampling, Nat. Photon. **11**, 361 (2017).

[24] H. Wang, J. Qin, X. Ding, M.-C. Chen, S. Chen, X. You, Y.-M. He, X. Jiang, L. You, Z. Wang, C. Schneider, J. J. Renema, S. Höfling, C.-Y. Lu, and J.-W. Pan, Boson sampling with 20 input photons and a 60-mode interferometer in a 10^{14}-dimensional hilbert space, Phys. Rev. Lett. **123**, 250503 (2019).

[25] J.-P. Li, J. Qin, A. Chen, Z.-C. Duan, Y. Yu, Y.-H. Huo, S. Höfling, C.-Y. Lu, K. Chen, and J.-W. Pan, Multiphoton graph

states from a solid-state single-photon source, ACS Photon. **7**, 1603 (2020).

[26] S. Chen, L.-C. Peng, Y.-P. Guo, X.-M. Gu, X. Ding, R.-Z. Liu, J.-Y. Zhao, X. You, J. Qin, Y.-F. Wang, Y.-M. He, J. J. Renema, Y.-H. Huo, H. Wang, C.-Y. Lu, and J.-W. Pan, Heralded three-photon entanglement from a single-photon source on a photonic chip, Phys. Rev. Lett. **132**, 130603 (2024).

[27] M. Valeri, P. Barigelli, B. Polacchi, G. Rodari, G. D. Santis, T. Giordani, G. Carvacho, N. Spagnolo, and F. Sciarrino, Generation and characterization of polarization-entangled states using quantum dot single-photon sources, Quantum Sci. Technol. **9**, 025002 (2024).

[28] H. Cao, L. M. Hansen, F. Giorgino, L. Carosini, P. Zahálka, F. Zilk, J. C. Loredo, and P. Walther, A photonic source of heralded GHZ states, Phys. Rev. Lett. **132**, 130604 (2024).

[29] J. H. Weber, B. Kambs, J. Kettler, S. Kern, J. Maisch, H. Vural, M. Jetter, S. L. Portalupi, C. Becher, and P. Michler, Two-photon interference in the telecom c-band after frequency conversion of photons from remote quantum emitters, Nat. Nanotechnol. **14**, 23 (2019).

[30] X. You, M.-Y. Zheng, S. Chen, R.-Z. Liu *et al.*, Quantum interference with independent single-photon sources over 300 Km fiber, Adv. Photon. **4**, 066003 (2022).

[31] L. Zhai, G. N. Nguyen, C. Spinnle, J. Ritzmann, M. C. Löbl, A. D. Wieck, A. Ludwig, A. Javadi, and R. J. Warburton, Quantum interference of identical photons from remote GaAs quantum dots, Nat. Nanotechnol. **17**, 829 (2022).

[32] K. A. Fischer, K. Müller, K. G. Lagoudakis, and J. Vučković, Dynamical modeling of pulsed two-photon interference, New J. Phys. **18**, 113053 (2016).

[33] K. A. Fischer, L. Hanschke, J. Wierzbowski, T. Simmet, C. Dory, J. J. Finley, J. Vučković, and K. Müller, Signatures of two-photon pulses from a quantum two-level system, Nat. Phys. **13**, 649 (2017).

[34] J. Iles-Smith, D. P. S. McCutcheon, A. Nazir, and J. Mørk, Phonon scattering inhibits simultaneous near-unity efficiency and indistinguishability in semiconductor single-photon sources, Nat. Photon. **11**, 521 (2017).

[35] A. Javadi, N. Tomm, N. O. Antoniadis, A. J. Brash, R. Schott, S. R. Valentin, A. D. Wieck, A. Ludwig, and R. J. Warburton, Cavity-enhanced excitation of a quantum dot in the picosecond regime, New J. Phys. **25**, 093027 (2023).

[36] J. Johansson, P. Nation, and F. Nori, QuTiP 2: A Python framework for the dynamics of open quantum systems, Comput. Phys. Commun. **184**, 1234 (2012).